Progress In Electromagnetics Research, Vol. 113, 285–312, 2011

WIDEBAND SOUNDER FOR DYNAMIC AND STATIC WIRELESS CHANNEL CHARACTERISATION: URBAN PICOCELL CHANNEL MODEL

D. L. Ndzi, K. Stuart, S. Toautachone, B. Vuksanovic and D. Sanders

Microwave Telecommunication Systems Research Group
Department of Electronic and Computer Engineering
University of Portsmouth, Anglesea Building
Anglesea Road, Portsmouth, PO1 3DJ, UK

Abstract—This paper presents a high speed configurable FPGA-based wideband channel sounder with signal bandwidths up to 200 MHz and results of a study of dynamic urban picocell channel. The use of FPGA allows the sounder to be adaptable for measurements in different scenarios. Adaptable options include changes to the waveform, bandwidth, channel sampling rate and real-time averaging to improve signal-to-noise ratio in weak signal conditions. The implemented architecture has led to a 60% reduction in size and weight compared to sounders in use elsewhere making it ideal for mobile channel measurements. The study of an urban picocell channel has shown that dynamic variation due to automotive traffic introduces average signal fades of up to 5 dB but causes frequency selective fading with depths of up to 40 dB. Existing channel models assume antenna heights of more than 6 m and path lengths of more than 30 m. Therefore there is a need for shorter path models and this paper proposes a linear picocell channel model for static and dynamic urban environment.

1. INTRODUCTION

Growth in wireless communication use has seen a shift in telecommunication pricing model from connectivity to data rate and quality of service model. The widespread use of smart-phones has also accelerated growth in high data rate applications. Significant

Received 29 December 2010, Accepted 31 January 2011, Scheduled 4 February 2011
Corresponding author: David L. Ndzi (david.ndzi@port.ac.uk).

studies have been carried out in short-range indoor environment [1, 2]. However studies in short-range outdoor environment where most of the mobile devices are used have received relatively little attention. In outdoor urban environment many studies have focused on macrocells [3].

Substantial research activities have produced numerous models relating to a variety of wireless channels [4–10]. In outdoor urban environment, a number of scenarios have been developed which can be broadly categorised as over roof-tops with static or mobile receivers for path lengths that are greater than 100 m [11–13]. In fixed wireless access channel models [14] where the transmitter and the receiver are static, the transmitter to receiver distance is too large. In addition to these, for distances less than 20 m most models, including the COST231-Walfisch-Ikegami-Model (COST231-WI), assume free-space path loss [15, 16]. The antenna heights and distances are not typical of current and future high data rate wireless access system set ups [17, 18].

Urban channels exhibit both spatial and temporal variations. Studies of induced dynamic variations in the channels due to movements within the urban picocell areas are limited. References can be found for indoor channels in [19–22]. Temporal variation of the channel can have significant impact on the performance of wireless systems resulting in a burst of errors in digital systems. Therefore, there is a need to understand the temporal variability of the channel response in order to assess its impact on wireless data rates [23]. Considerable studies have been carried out using Multiple-Input Multiple-Output (MIMO) systems resulting in a large number of publications of MIMO channel models [24]. A large study of spatial channels with path lengths, mainly, from 30 m up to 8 km have also been undertaken under the 3GPP group for bandwidths of 5 MHz [25]. This has been extended by the WINNER project for bandwidths up to 100 MHz and a number of models have been proposed for a range of communication channels in urban and suburban environment [26].

The diversity of the urban environment and the dynamic nature of the channels make the measurement and analysis approach critical to ensure that results obtained are representative and can be applied to similar channels. Wideband channel sounders are often used to study broadband wireless channels. Channel sounding take many forms and the systems that are used have evolved in parallel with the interest in wireless communication [27–29]. Some techniques, such as pulse or frequency swept transmissions, have been widely used in many measurement studies [30–34]. Although simple to construct and low cost, these techniques suffer from poor multipath delay resolution and slow channel measurement rates. These make

their use in the investigation of fast dynamic channels impractical. When the received signal is digitised, the hardware complexity becomes disproportionately high due to the spectral inefficiency of the signals [35, 36].

Sounders based on the cross-correlation techniques have been widely used over the years [37–41]. In this technique the received signal is correlated with an identical transmitted sequence clocked at a slower rate or at the same rate as in the transmitter but such that the two sequences pass each other on a step-by-step basis rather than continuously. Digital frequency synthesisers have also been used with this technique to increase signal bandwidth, multipath resolution and channel sampling speed. However the use of waveforms such as phase codes and Chirp increases the complexity of the receiver [42].

Multitone channel sounders have recently become practical with the advent of technology that enables complex waveform generation [43]. Channel sounders that use multitone waveforms have many advantages over other systems because of the spectral efficiency of the waveforms which reduce hardware complexity. Further advantages include the ability to operate without carrier acquisition and code/carrier recovery circuitry, which is necessary when a Chirp signal is used. However these systems require experience and expertise to construct and are often expensive to purchase making them unaffordable for most organisations.

There are a number of other channel sounders of differing architectures that are commercially available [43–46]. In general channel sounders are expensive, big and heavy with complex receiver architectures. There are other channel sounding techniques that are comparatively cheaper to implement [47, 48], although with limited channel resolution, sampling rate and sensitivity. These highlighted the need for the development of a simpler architecture that can be adapted for different studies [49].

In this paper, the development of an adaptable wideband channel sounder with signal bandwidths up to 200 MHz based on the transmission of a Pseudo Random Gaussian Noise (PRGN) waveform is presented. The objective of the development was to build a system which is compact and yet adaptable that addresses the problem of restricted mobility, speed, range restriction and cost inherent in many channel sounders. The sounder is designed to be configured to implement real-time processing of data that improves the Signal-to-Noise Ratio (SNR) by up to 30 dB in weak signal conditions. Channel sampling rates up to 5.4 kHz can be achieved. This paper also presents results of urban channel measurements designed to investigate spatial channel variation over short path distances and temporal variations

induced by automotive traffic. The processing approach used allows the detection of induced channel variation as vehicles pass in close proximity of the transmitter to receiver path, although they do not traverse the path. The study is of benefit to researchers, system designer and network providers who are working on the optimisation of data rates and provision of wideband services in urban environment. The papers is organised as follows; Section 2 describes the wideband channel sounder that has been developed. The design objectives, implementation and tests carried out to evaluate the performance of the sounder are provided. Spatial and temporal channel variation measurements are described in Section 3. This is followed by the results of signal variations, analysis and description of a picocell outdoor urban channel model in Section 4.

2. SYSTEM DESCRIPTION

The objective of the new sounder design was to overcome the limitations of channel sounders in use, in general. Thus the design objective was: *"to developed a very compact, low cost and adaptable sounder to measure the channel transfer function of a channel, over the widest possible bandwidth in the shortest possible time and as often as possible with the ability to improve the channel signal-to-noise ratio"*. This rendered most of the channel sounding implementation techniques unsuitable.

The approach adopted in the development of the channel sounder uses a synthesized multitone waveform called PRGN [50]. Field Programmable Gate Array (FPGA) technology has been used, in preference to Digital Signal Processors, to minimise the number of discrete components in the system, enable adaptability and provide real-time data processing capability [51–53]. The PRGN characteristics include a rectangular spectrum which allows sampling to be carried out at exactly the Nyquist frequency thereby minimising the complexity of the receiver system.

2.1. Transmitter

The transmitter is made up of an Arbitrary Waveform Synthesizer (AWS) and a Radio Frequency (RF) unit. The dual channel AWS generates a PRGN signal with an optimised crest factor which has a flat amplitude spectrum and low sidelobes outside the desired bandwidth. The AWS can generate two independent simultaneous waveforms with bandwidths of up to 150 MHz from channel A and 200 MHz from channel B, a capability that is important for co-located

channel investigation. However for the study reported in this paper only channel B was used. A simplified block diagram and the image of the AWS that has been developed are shown in Figure 1. The PRGN waveform used consists of 1024 spectral lines with 195.313 kHz frequency resolution over a bandwidth of 200 MHz [50]. The DAC is driven by a 400 MHz clock generated using FPGA from a 10 MHz input reference clock. The 200 MHz PRGN time and frequency domain signal that is generated by the AWS is shown in Figure 2. The transmitter unit has been built to transmit at a carrier frequency of 2 GHz. The use of a phase-locked 10 MHz reference signal that can be locked to a GPS receiver eliminates the transmitter and receiver synchronisation problem inherent in most channel sounding techniques. A simplified block diagram of the transmitter and an image of the built system are shown in Figure 3.

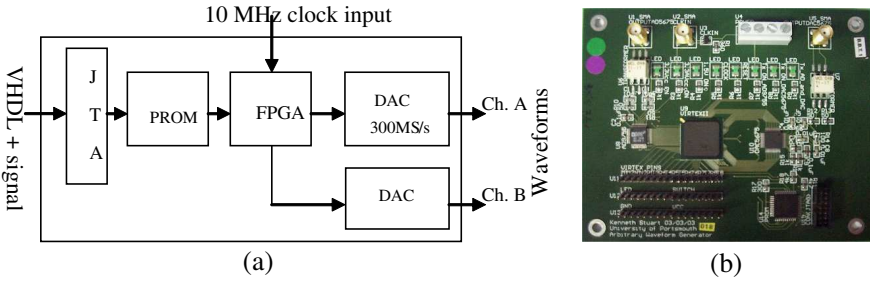

Figure 1. (a) Simplified block diagram and (b) image of the arbitrary waveform synthesizer card (10×12 cm).

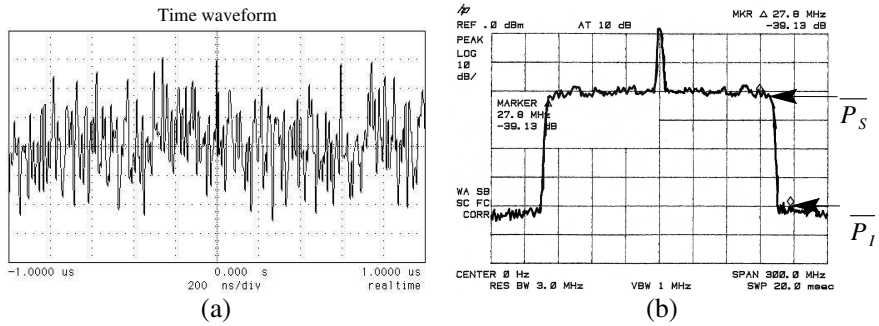

Figure 2. (a) PRGN time domain signal and (b) frequency magnitude spectrum generated by the AWS.

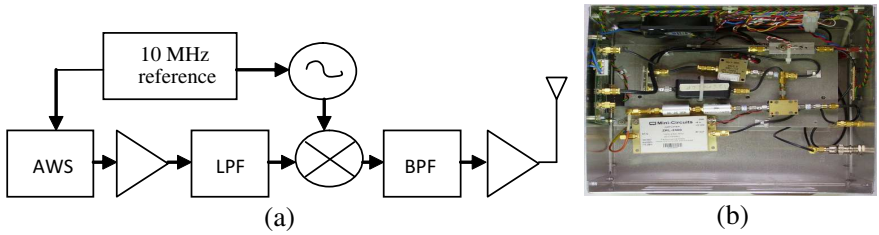

Figure 3. (a) Simplified block diagram and (b) the realised transmitter unit.

2.2. Receiver

The receiver system is comprised of a RF unit, a 12-bit resolution Analog-to-Digital Converter (ADC) [54], ADC carrier card, PCI Mezzanine Card (PMC) [55, 56] and a computer. A simplified block diagram of the receiver unit, ADC carrier card and built receiver unit is shown in Figure 4. The ADC has sampling rates up to 400 MS/s and is used to sample the signal at an Intermediary Frequency (IF). The sampled data is output through two channels thereby halving the frequency. The PMC card is used to implement real-time averaging of the sampled data using FPGA. The data is transferred to the computer

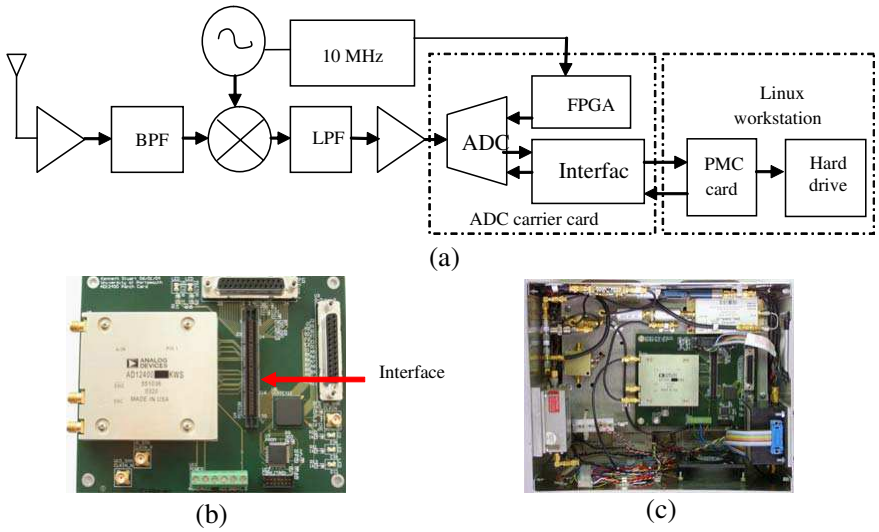

Figure 4. (a) Simplified block diagram of the receiver unit, (b) ADC carrier card and, (c) receiver unit.

across the PCI data bus for storage using demand-mode direct memory access. The acquisition time for each channel measurement (without averaging) is 10.24 µs. The user can select the number of real-time averages to be preformed up to 1024. This gives a theoretical improvement in SNR of between 3 dB and 30 dB. A block diagram of the averaging process and the PMC is shown in Figure 5 and illustrates how First-In-First-Out (FIFO) memory blocks are used in the averaging process.

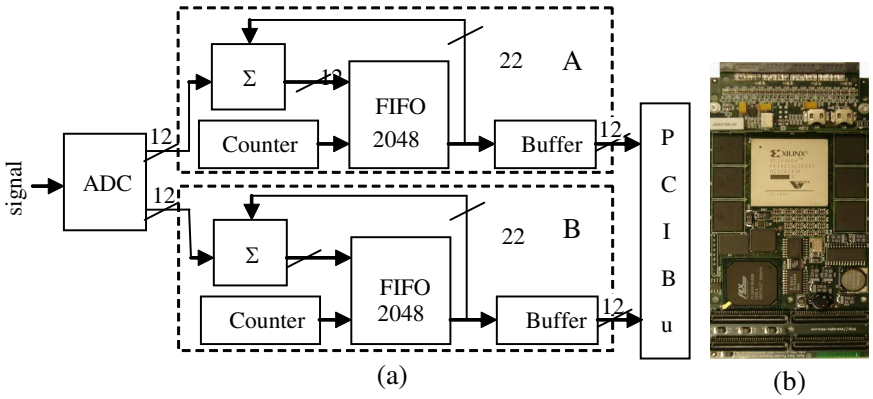

Figure 5. (a) Simplified block diagram of averaging unit and, (b) PCI Mezzanine Card.

2.3. Data Acquisition and Real-time Averaging

The developed software allows the user to implement a data acquisition strategy that optimises the speed of channel measurements, the amount of captured data and signal-to-noise ratio for the channel under investigation. It provides the flexibility for the user to control the data acquisition strategy by changing:

- the number of real-time averages to be carried out;
- time gap between successive channel transfer function measurements;
- time gap between a continual block of successive measurements;
- the number of data files to be captured and hence, the duration of the measurements; and
- when configured in conjunction with the transmitter, the bandwidth and sequence length of the waveform.

Periodic averaging is performed in real-time on the PMC card. This helps to reduce the amount of data that needs to be transferred across the PCI bus.

Tests were carried out to determine the sustainable data rates from the ADC to the computer hard drive. They revealed that the average PCI bus data rate was 55.7 MB/s and the average hard disk write speed was 40 MB/s. When sampling at 400 MS/s, the ADC generates 600 MB of data per second. With a hard disk write speed of 40 MB/s, 15 times reduction in data rate is required from the ADC to the computer hard disk. This can be achieved as a consequence of performing real-time averaging. The time taken to capture one averaged snapshot, T_{as}, is given by Equation (1).

$$T_{as} = \frac{N_s N_a}{2 f_c} + T_{sg} \tag{1}$$

where N_s is the sequence length, N_a is the number of averages, T_{sg} is the time required to reset the counters and FIFO, and f_c is the sampling frequency in Hz. Due to timing constraints when using clock frequencies greater than 390 MHz, T_{sg} has been set to a minimum value of 20.48 µs. The quantity of data generated for each value of N_a is shown in Table 1. It shows that data can be captured continually for number of averages greater than 16. For number of averages less than 32, the quantity of data per second must be limited to 40 MB. This can be achieved by increasing the time gap (T_{sg}) between each snapshot or continual measurements such that the number of channel responses captured per second is less than 4882.

With a 200 MHz bandwidth, the FPGA device speed grade used on the PMC card is operating at a frequency that is close to its limit. Thus, for different numbers of averages, the design had to be individually optimised. This could be alleviated by using a faster FPGA device. Fully adaptable data acquisition software has therefore been developed for all number of averages, up to 1024, at bandwidths up to 180 MHz. For 200 MHz bandwidth, the sounder has been designed to be adaptable for 1, 16 and 1024 averages. Table 2 provides details of the timing parameters for each number of averages (N_a) for 200 MHz signal bandwidth transmission.

The following terms are used to describe the data:

- snapshot: — a complete sequence (4096 sample long) of the PRGN waveform;
- averaged snapshot: — a complete sequence (4096 sample long) produced from the averaging process;
- data block: — 240 snapshots (averaged or not);
- data file: — 4 data block.

Table 1. Number of averages, time to capture one channel response and volume of data generated per second.

N_a	T_{as} ms	No. of snapshot per second	Data generated per second (MB)
1	0.03072	97656	266.666
2	0.04096	48828	200.000
4	0.06144	24414	133.333
8	0.10240	12207	80.0000
16	0.18432	6103	44.4444
32	0.34816	3051	23.5294
64	0.67584	1525	12.1212
128	1.33120	762	6.15385
256	2.64192	381	3.10076
512	5.26336	190	1.55642
1024	10.5062	95	0.77972

Table 2. 200 MHz bandwidth data acquisition; number of averages, theoretical improvement in SNR and timing.

N_a number of averages	Theoretical ΔSNR dB	T_{as} (ms)	Channel sampling rate (Hz)
1	0	0.18432	5425
16	12	0.18432	5425
1024	30	10.5062	95

The user can increase the number of averages (N_a), the time between snapshots (T_{sg}), and the time between data block (T_{dbg}) to suit the environment under investigation. The resulting time to capture one averaged snapshot (T_{as}), one data block (T_{db}) and one data file (T_{df}) can be calculated using Equations (1), (2) and (3), respectively.

$$T_{db} = 240T_{as} + 239T_{sg} \tag{2}$$

$$T_{df} = 4T_{db} + 3T_{dbg} \tag{3}$$

where,

$$T_{sg} = T_{dbg} = N_g \left(\frac{2N_s}{f_c} \right) \tag{4}$$

and N_g is the number of multiples of the time taken to reset all counters and FIFOs used in the averaging process. T_{sg} and T_{dbg} are independent of each other.

For a 200 MHz bandwidth signal the values of T_{sg} and T_{dbg} are given by Equations (5) and (6).

$$T_{sg} = 2T_s \tag{5}$$

$$T_{dbg} = 0.2517 - T_{db} \tag{6}$$

2.3.1. Data Processing and Calibration

Before the channel parameters can be estimated, each transfer function is first down converted to baseband and calibrated to remove the system response (magnitude and phase). These operations are done in software. The down-conversion of the signal from IF to baseband is realised by multiplying each sample of the measured sequence by conceptual orthogonal phased oscillators for in-phase (7) and quadrature-phase (8).

$$f_{loI} = \sin\left(\frac{2\pi f_c}{4}\right) \tag{7}$$

$$f_{loQ} = \cos\left(\frac{2\pi f_c}{4}\right) \tag{8}$$

The local oscillators (f_{loI} and f_{loQ}) are required to be one quarter of f_c, for down-conversion of the in-phase and quadrature-phase channels.

Each transfer function is then calibrated using a reference transfer function measured with the channel sounder in an anechoic chamber. The configuration of the measurement set-up used is shown in Figure 6.

From Figure 6, the relationship between the input PRGN waveform, S_{PRGN}, and the calibrated output, G_{mea}, is given by,

$$G_{mea} = S_{PRGN}\left(H_{Tx}H_{ant}H_{channel}H_{ant}H_{Rx}H_{spu}H_{cal}\right) \tag{9}$$

If a reference transfer function measured from the channel is G'_{ref}, and the corresponding ideal calibrated channel transfer function is H'_{ref}, then,

$$G'_{ref} = S_{PRGN}\left(H_{Tx}H_{ant}H'_{ref}H_{ant}H_{Rx}H_{spu}H_{cal}\right) \tag{10}$$

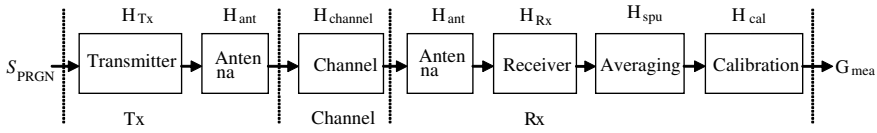

Figure 6. Configuration for calibration measurements.

Dividing (9) by (10) gives,

$$\frac{G_{mea}}{G'_{ref}} = \frac{H_{channel}}{H'_{ref}} \tag{11}$$

Since, H'_{ref} represents an ideal channel response measured under high SNR condition and exhibits a flat spectrum, therefore,

$$\frac{H_{channel}}{H'_{ref}} \approx H_{channel} \tag{12}$$

All system responses (magnitudes and phases) are eliminated and the transfer function, $H_{channel}$, represents only the response associated with the measured channel.

2.4. System Tests and Evaluation

Exhaustive tests were carried out to assess the functions and capability of the sounder. The transmitter and receiver RF units were designed to optimise the power sensitivity of the receiver and minimise intermodulation products. In order to achieve this, measurement of input and output power, and signal to intermodulation product ratios were evaluated at every stage in the RF chain.

An example of the 200 MHz PRGN spectrum at the output of the AWS is shown in Figure 2(b). The arbitrary waveform contains 1024 discrete spectral lines in the range ±100 MHz with a frequency resolution of 195.313 kHz. The noise power associated with the waveform is defined by the Signal-to-Intermodulation Ratio (SIR) or the SNR. The total signal power (P_s) of the waveform is given by,

$$P_S = \sum_{i=1}^{1024} \overline{P_S} = 1024\overline{P_S} \tag{13}$$

where $\overline{P_S}$ is the mean level of the wideband signal components.

Intermodulation products are coherent and hence cannot be minimised by periodic averaging of the signal. The total power of the intermodulation products and noise is given by,

$$P_I = \int_0^{B_w} \overline{P_I(f)} df \tag{14}$$

where $\overline{P_I(f)}$ is the mean level of any intermodulation components and/or noise at all frequencies within the bandwidth. Since it is not possible to separate intermodulation products from noise, the estimated mean level of the components represents an equivalent

Signal-to-Intermodulation and Noise Ratio (SINR). Thus, the SINR can be expressed as,

$$SINR = 10 \log \left(\frac{P_S}{P_I} \right) \tag{15}$$

If the value shown in Figure 2(b) is assumed to be the mean level of the intermodulation components plus noise, the estimated SINR is 39 dB. The transmitted power is 21 dBm. Figure 7 shows the PRGN spectrum at the input of the ADC. The SINR is 28 dB. Without averaging, the sensitivity of the receiver is −81 dBm.

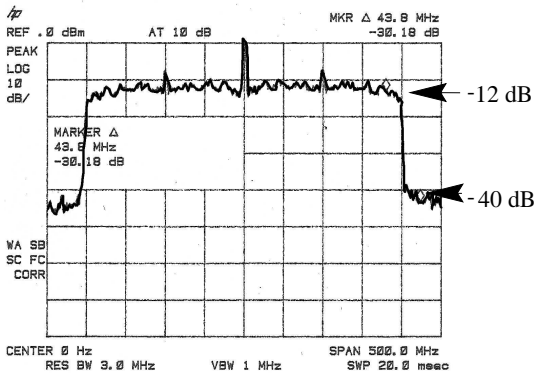

Figure 7. PRGN at the input to the ADC in the receiver.

2.4.1. Simulation of Channel Fading

Back-to-back tests were conducted to assess the performance of the system under simulated flat fading and frequency selective fading conditions using the set-ups shown in Figure 8. The delays and magnitudes of the signals in the primary and secondary paths were controlled using attenuators and different lengths of semi-rigid cables. Figure 9 shows a photo of the laboratory set-up. Comparisons were made between the measured improved SNR and the theoretical values.

Figures 10 and 11 show the measured transfer functions with 1 (no averaging) and 16 averages for flat fading and frequency selective fading channels, respectively. The magnitude response of the system was not calibrated out and can be seen in the spectrum. For frequency selective fading, a 2-ray model was simulated.

The magnitudes of the components between the spectral lines in the transfer function represent the level of noise plus any intermodulation products. The estimated SINR is 23.4 dB, Figure 10.

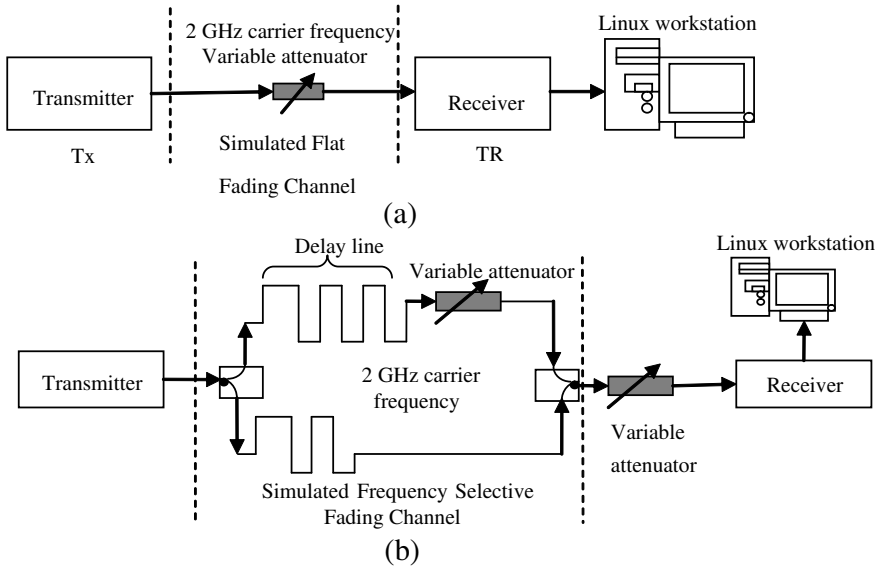

Figure 8. Set-up for (a) flat fading and, (b) frequency selective fading channel simulation.

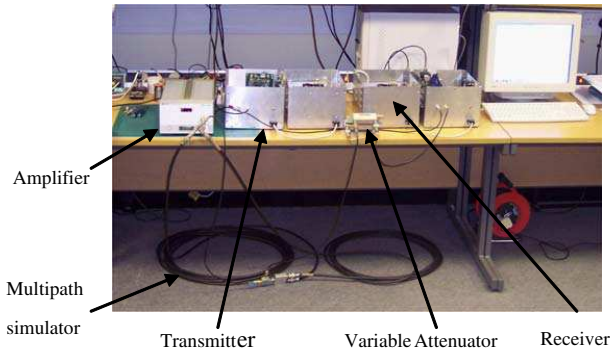

Figure 9. Configuration of hardware for multipath simulation.

An improvement in SNR of 11.2 dB is achieved with 16 averages which is 0.8 dB below the theoretical value of 12 dB. Figure 11(b) shows that the processing gain enables the depth of the fade nulls within the bandwidth to be determined.

Figure 12 shows the improvement in SNR for averages up to 1024 compared to the theoretical values. An improvement of 12.2 dB was achieved with 32 averages, which is 2.8 dB below the theoretical value.

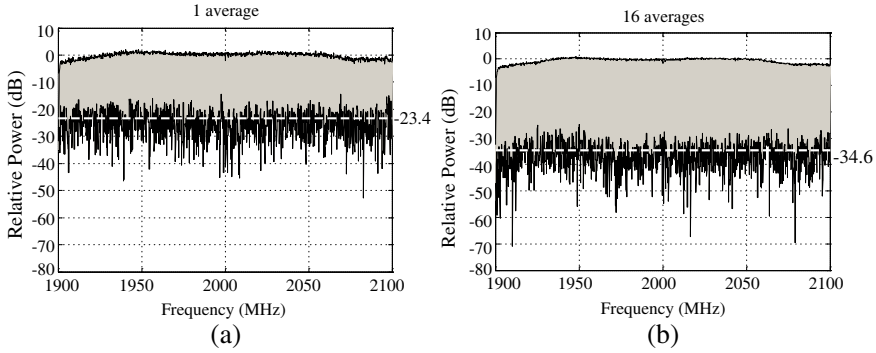

Figure 10. Transfer function of simulated flat fading channel with; (a) 1 averages and, (b) 16 averages.

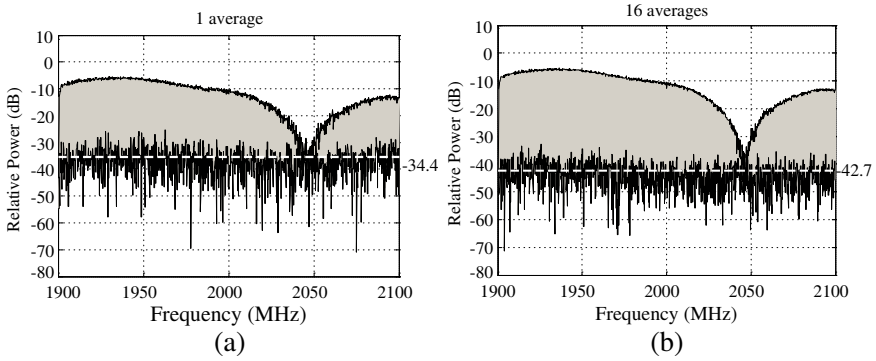

Figure 11. Transfer function of simulated 2-ray multipath channel with: (a) 1 averages and, (b) 16 averages.

For higher number of averages, the measured SINR improvement flattened out at approximately 18.6 dB for $N_a = 1024$. Since any intermodulation components present are coherent, signal averaging will only be effective in integrating out the noise. Therefore, the differences in levels between the SINRs for different number of averages represent the corresponding improvement in SNR. In addition, the theoretical improvement in SNR assumes that the noise is white Gaussian uncorrelated noise.

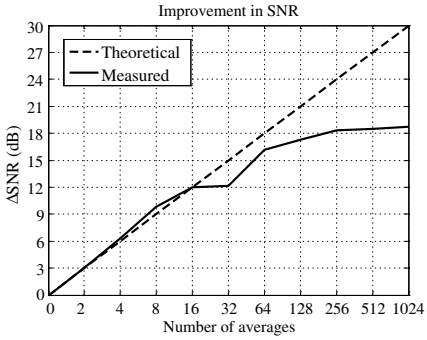

Figure 12. Comparison of theoretical and measured improvements in SNR for different number of averages.

3. CHANNEL MEASUREMENTS

In an outdoor wireless environment, the movement of people, objects and vehicles cannot always be controlled. The movement and, hence, position of the user and surrounding objects will vary and introduce both spatial and temporal variations. To study these changes, measurements were conducted in a position typical of an urban high data rate wireless access hotspot. For long range or wide area coverage transmissions, little or no attention is paid to short paths variations. However as cell sizes have reduced, the ability to accurately characterise path loss over specific short distances has become more important than general models over larger distances, particularly in high data rate wireless access environments.

Measurements were carried out in front of a building (Anglesea Building) which is adjacent to a dual carriage road in an urban area. The environment is typical of an urban area with relatively high number of mobile wireless communication users and hence, a most likely position for a high speed access hotspot. The area is also similar in size to a bar, cafe or shop front where WLAN access points are widely used. The speed at which the vehicles travel is typically between 20 and 45 km/h and the distance of the traffic from the transmitter to receiver path ranges from 3.5 m to 15.1 m. The number of vehicles travelling in both directions varied throughout the measurement period. Figure 13 provides an illustration of the routes and, the positions of the transmitter and receiver.

Video recordings synchonised with the channel measurements were made and used to corroborate the signal variations observed. The transmitter antenna height was 2.5 m and the receiver antenna height was 1.6 m. Omni-directional antennas were used.

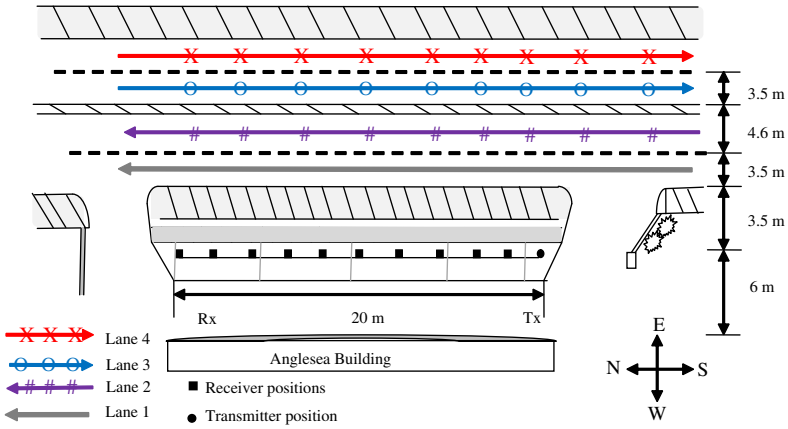

Figure 13. Measurement Set-up.

The distance between the transmitter and receiver was increased from 2 m to 20 m in steps of 0.3 m parallel to the direction of traffic. At each receiver position, the channel was sampled for approximately 20 s, that is 19200 channel response measurements. Figure 14 shows an example of the transmitter and receiver positions.

Figure 14. Transmitter and receiver position during measurement.

4. MEASUREMENT RESULTS

Observed temporal variations at each position were induced by moving objects, vehicles, and not due to the movement of the transmitter or receiver. In addition, no vehicles cross the transmitter to receiver path during the study.

Figure 15 shows an example of signal power variation with time and the impact of a vehicle on received signal. It shows that multipath

components introduce significant variations in the signal levels with deep fades. Figure 16 shows the channel transfer functions and corresponding impulse responses when no vehicle was passing (static

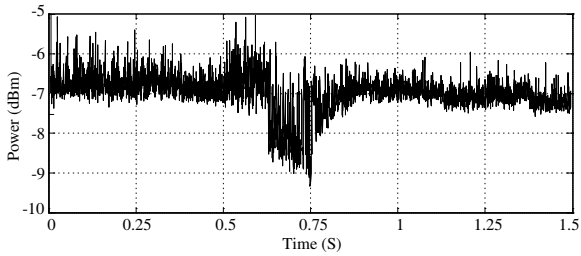

Figure 15. Averaged received power.

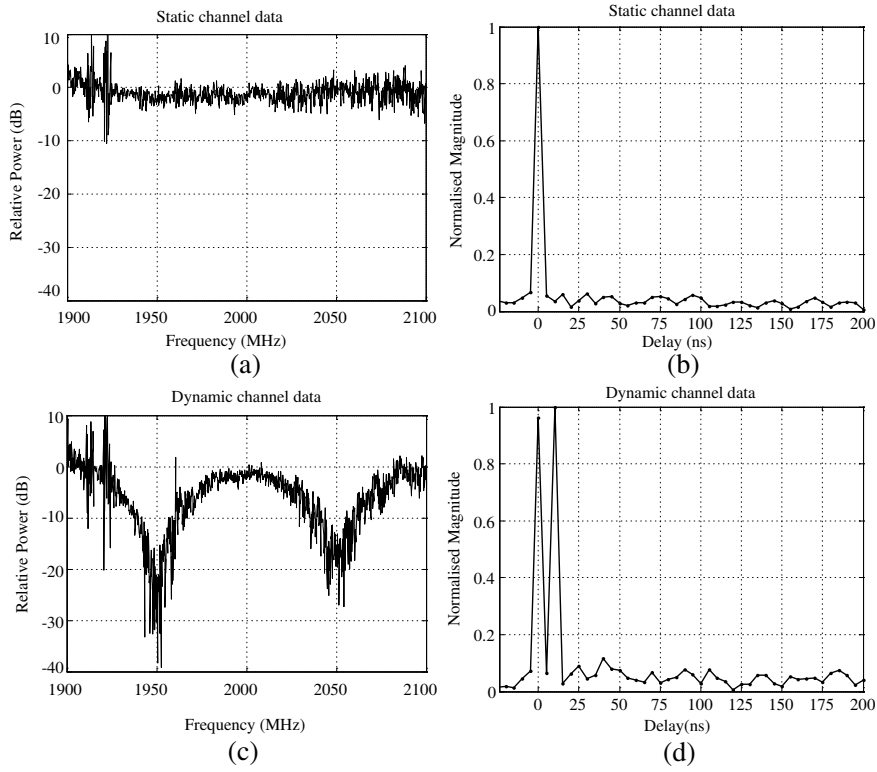

Figure 16. Field measurements (a) transfer function and, (b) impulse response with no vehicles, and (c) transfer function, and (d) impulse response with a vehicles passing.

channel) and when there was a vehicle travelling parallel to the transmitter to receiver path. The static channel transfer function (Figure 16(a)) exhibits small variations and very small fade depth. However, the dynamic channel response shows rapid fading with large fade depths due to multipath of up to 40 dB. The position of the nulls within the bandwidth changes with vehicle position and direction due to changes in the time delay of the multipath components. The impulse response from the static channel shows only one dominant path, Line-Of-Sight (LOS) path, as would be expected (Figure 16(b)). However, when a vehicle is passing, the multipath component is very strong (Figure 16(d)). Figure 15 shows smaller amplitude variations than fade depths observed within the bandwidth because it is the average signal power across the bandwidth which masks the severity of frequency selective fading within the channel. The measured fade depths are similar to results reported in [57].

A section of averaged received power is shown in Figure 17 and the vehicles that were captured on video passing through the measurement zone are indicated. The video recording showed that the speed of traffic was between 30 km/h and 45 km/h. As the first vehicle in Figure 17 (3 door estate) moved through, the results show that the fade duration was approximately 30 ms. Examination of the data file showed that the start of the event was not captured but data acquisition did continue until the vehicle had left the measurement zone. The last vehicle to pass was an estate car which was travelling in Lane 4 (Figure 13). Results show that longer vehicles have longer lasting effects on the received signal. An increase in the transmitter to receiver path length also increases the duration of the fading. When the path length was reduced to less than 6 m, the duration of the effects of vehicles on the channel was also reduced.

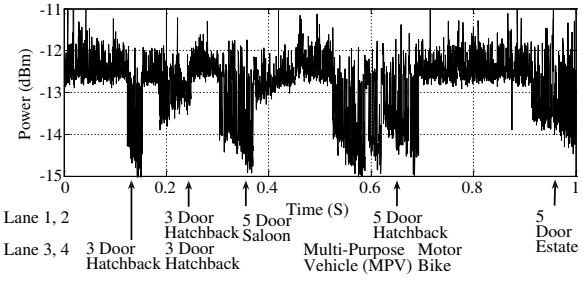

Figure 17. Averaged received power showing the impact of reflections from vehicles (Tx-Rx distance: 12 m).

Considering the average signal power across the bandwidth, the presence of a vehicle in the channel introduces fade depths of up to 4 dB. Because the vehicle is not traversing the transmitter to receiver path, the decrease in the signal power is due to multipath fading caused by scattered and reflected components. There is also an increase in the standard deviation of the averaged signal power in the presence of traffic. A further increase was observed as the number of vehicles increased.

4.1. Path Loss Model

Most of the models published in open literature for urban environments are either for path lengths greater than 1 km or assumptions have been made about the prevailing propagation mechanisms. Models based on prevailing propagation mechanisms cannot be directly applied to this study because they are based on work in which the transmitter heights were greater than 10 m or the systems used transmitted narrow band signals or very few measurements were taken at antenna separations less than 30 m.

The models published for short path lengths include the COST231-Walfisch-Ikegami and Wideband Microcell (WM) [58, 59]. They proposed a log-distance model. The COST231-Walfisch-Ikegami model uses free-space for distances less than 20 m and assumes transmitter antenna heights between 4 and 50 m. The model is described by (16). The WINNER project model for urban microcell is described by (17) [26].

$$PL_{COST231\_W} = 42.6 + 26\log_{10} d\,[\text{km}] + 20\log_{10} f_c\,[\text{MHz}] \quad (16)$$

$$PL_{WINNER} = A\log_{10} d\,[\text{m}] + C\log_{10}\left(\frac{f_c\,[\text{GHz}]}{5}\right) + B \quad (17)$$

where d is the distance between the antennas and f_c is the carrier frequency. For urban microcell environment (WINNER B1), the values of $A = 22.7$, $B = 41.0$ and $C = 20$ and, the transmitting antenna is assumed to be below surrounding buildings roof tops and in LOS. The model has been developed to be valid for antenna separations from 10 m. The values of $A = 13.9$, $B = 64.4$ and $C = 20$ have been proposed for indoor channel (WINNER B3)for base station antenna height of 6 m and mobile antenna height of 1.5 m for distances between 5 m and 100 m.

In this study, to evaluate the channel models, the data was separated into measurements in the presence of traffic (dynamic) and measurements when there was no vehicle passing (static). The results of signal variation with distance are presented in Figure 18. They show

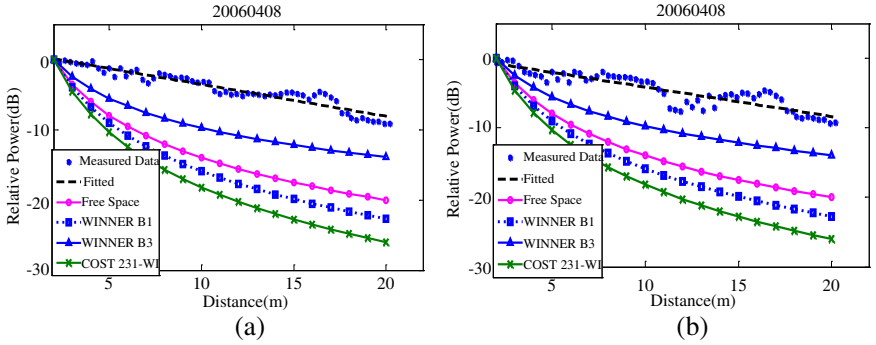

Figure 18. Signal variation with distance for (a) static and, (b) dynamic channels.

that at ranges up to 20 m none of the channel models closely represents the signal variation with distance. It was found that a linear model provides a best fit. The signal loss with increased distance did not decay logarithmically as predicted by the models.

Because of the short path length and absence of clutter, the received signal was dominated by the LOS path. In the absence of automotive traffic, multipath components were very weak. Linear path loss was also obtained during dynamic channel variation, as shown in Figure 18(b). However greater variations of signal power which depended on the size, number and direction of vehicles passing were observed. In general, the gradient of the path loss for each measurement scenario was less than the values predicted by free space path loss, WINNER and COST231-Walfisch-Ikegami models over short path lengths.

4.1.1. Small-scale Variations

Small-scale variations of the signal have been computed from measurement results. This has been used to calculate the signal power distribution about its mean, across the bandwidth, in a narrow band sense.

Results show that for dynamic channels, for path lengths up to 10 m, signal variation is best described by a Rician distribution. However in a static channel the signal variation is best described by a Normal distribution. Figure 19 shows results from measurements at an antenna separation of 8 m. At large antenna separations the small-scale variations of a dynamic channel have been found to be best described by a Nakagami distribution. Nakagami distribution

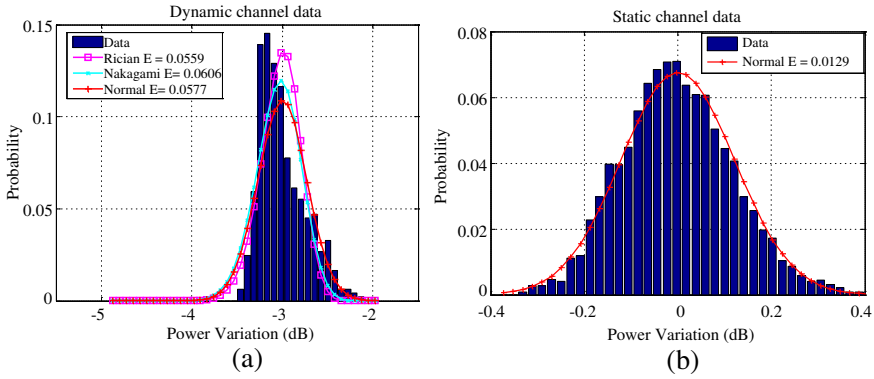

Figure 19. Small-scale variation: (a) dynamic channel, (b) static channel.

has Rice and Rayleigh distributions as extreme cases. The change in statistical distribution with path length in the presence of traffic can be attributed to an increase in multipath components due to reflection and scattering. However, for measurement conducted in static environment Normal distribution still gives the best results. Figure 20 shows typical results from measurements at 20 m.

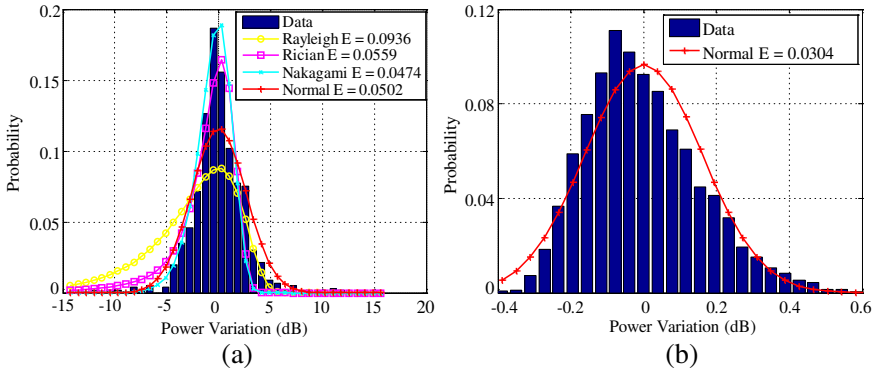

Figure 20. Small-scale variation: (a) dynamic channel, and (b) static channel.

The signal power variations at short path lengths up to 10 m showed that moderate variations about the mean in a static channel was generally within 2 dB. Overall an increase in signal variations with antenna separations was observed due to greater contributions from scattered components. This was more significant in dynamic channels where standard deviation of up to 12 dB were obtained.

The gradient of the average signal power is -0.45 for static channel and -0.42 for a dynamic channel. The smaller gradient of dynamic channel is due to average signal level enhancement by multipath components. The picocell signal decay models for dynamic and static channels are given by (18) and (19) respectively.

$$L_{apD}(d) = -0.42d + P_0 \tag{18}$$

$$L_{apS}(d) = -0.45d + P_0 \tag{19}$$

where d is the distance in meters and P_0 is the signal power in dBm at the reference distance d_0. Given that the signal variation about the mean at each measurement position can be described by a statistical distribution, picocell channel models can be developed for static and dynamic urban environments. The resulting static channel model can be described using Equation (20);

$$L_S\,(\text{dB}) = p_{no}(x|x_a) + L_{apS}(d) \quad 2 \le d \le 20 \tag{20}$$

and the urban dynamic channel model by Equation (21).

$$L_D\,(\text{dB}) = \begin{cases} p_{ri}(x|x_a) + L_{apD}(d) & 2 \le d \le 10 \\ p_{na}(x|x_a) + L_{apD}(d) & 10 < d \le 20 \end{cases} \tag{21}$$

where $p_{no}(x|x_a)$, $p_{ri}(x|x_a)$ and $p_{na}(x|x_a)$ are the distributions describing the variation in signal power about the average power x_a at each position. The signal power distributions are defined as follows,

$$p_{no}(x|x_a) = \frac{1}{\sigma\sqrt{2\pi}} e^{-\left[\frac{(x|x_a-\mu)^2}{2\sigma^2}\right]} \tag{22}$$

$$p_{ri}(x|x_a) = \frac{(x|x_a)}{\sigma^2} e^{-\left[\frac{(x|x_a)^2+A^2}{2\sigma^2}\right]} I_0\left(\frac{(x|x_a)A}{\sigma^2}\right) \tag{23}$$

$$p_{na}(x|x_a) = \frac{2m^m}{\Gamma(m)\Omega^m}(x|x_a)^{2m-1} e^{-\frac{m}{\Omega}(x|x_a)^2} \tag{24}$$

where μ and σ are the mean and standard deviation of $(x|x_a)$; A is the amplitude of the LOS component, I_0 is the modified Bessel function of the first kind and zero order, Ω is the scale parameter equal to the mean value of $(x|x_a)^2$ and m is the Nakagami parameter.

5. CONCLUSIONS

A wideband channel sounder capable of capturing the evolving response of a rapidly changing radio link has been described. It uses a Pseudo Random Gaussian Noise waveform that has a rectangular spectrum and negligible side-lobes. This allows the receiver to sample the waveform at exactly the Nyquist frequency providing

better sampling efficiency compared to other waveforms e.g., Chirp. Configurable technology (FPGA) has been used which enables the sounder to be adapted for measurements in different scenarios by changing the waveform, bandwidth, channel sampling rate and number of real-time averages. The use of FPGA improves the reliability of the sounder and allows for compact design and future upgrades without changing the architecture. The problem of transmitter and receiver synchronisation has been eliminate by using frequency references that can be obtained from GPS receivers or similar transmissions thereby eliminating link path length restriction inherent in wideband channel measurements. Back-to-back test results have shown that the improvement in signal-to-noise ratio achievable with up to 16 periodic averaging in the presence of random Gaussian noise can be represented by $10 \log_{10} N_a$, where N_a is the number of averages.

One of the main contributions of this paper is that the developed channel sounder architecture has allowed a more than 60% reduction in the size, weight and cost of the channel sounder systems whilst providing more flexibility in channel measurement. The architecture has been used to shift channel sounder system complexity from hardware to software. The application of programmable technology allows advantages to be taken of future faster devices in channel characterisation without changing the fundamental architecture of the sounder.

Measurements carried out in an urban environment has shown that automotive traffic, although not bisecting the transmitter-to-receiver path, can introduce frequency selective fading of up to 40 dB. Results show that the duration of the fade and depth depend on the size of the passing vehicle. Although the fade depths within the bandwidth are large, the averaged received power across the bandwidth exhibits relatively smaller variations. This shows that the impact of dynamic variations on wideband signals within picocell environment is dominated by the quality of the signal rather than signal strength. The temporal nature of the impact of dynamic variation will introduce error burst in digital receptions.

Channel models for urban microcell and picocell have largely assumed large antenna heights and long path lengths. For small distances less than 20 m, free space path loss is assumed. Results from the study reported in this paper show that for path length up to 20 m a linear path loss model with a gradient that is less than 1 dB/m can be used. The results also show that path loss is smaller than predicted by the WINNER model for indoor channels (B3). Overall, in static conditions, the small scale signal variation can be modeled using a Gaussian distribution about the mean. However

under dynamic conditions, signal variation is Rician distributed for antenna separations up to 10 m and Nakagami distributed for antenna separations beyond 10 m. This paper has produced useful results relevant to system planning and design for urban picocell high data rate transmissions. In particular, the results are relevant to high data rate ad-hoc network systems which use short range transmissions.

REFERENCES

1. Ndzi, D. L., N. Savage, and B. Gremont, "Spatial and temporal variation of wideband indoor channels," *International Journal of Antennas and Propagation*, Vol. 2010, Article ID 735434, 11, 2010.
2. Ndzi, D., J. Austin, and E. Vilar, "Hyper-resolution indoor channel impulse responses: Multipath components and k-factors," *Electronics Letters*, Vol. 35, No. 9, 698–699, April 1999.
3. Maciel, L. R., H. L. Bertoni, and H. H. Xia, "Unified approach to prediction of propagation over buildings for all ranges of base station antenna height," *IEEE Transactions on Vehicular Technology*, Vol. 42, No. 1, 41–45, January 1993.
4. Kurner, T., D. J. Cichon, and W. Wiesbeck, "Concepts and results for 3d digital terrain-based wave propagation models: An overview," *IEEE Journal on Selected Areas in Communications*, Vol. 11, 1002–1012, September 1993.
5. Hashemi, H., "The indoor radio propagation channel," *IEEE Proceedings*, Vol. 81, No. 7, 941–968, July 1993.
6. Cichon, D. J. and T. Kurner, "Propagation prediction models," *COST 231 Final Report*, Chapter 4, 134, 1999.
7. Goncalves, N. C. and L. M. Correia, "A propagation model for urban microcellular systems at the UHF band," *IEEE Transactions on Vehicular Technology*, Vol. 49, No. 4, 1294–1302, July 2000.
8. Juan-Llacer, L., L. Ramos, and N. Cardona, "Application of some theoretical models for coverage prediction in macrocell urban environments," *IEEE Transactions on Vehicular Technology*, Vol. 48, No. 5, 1463–1468, September 1999.
9. Berg, J., "A recursive method for street microcell path loss calculations," *IEEE International Symposium on Personal, Indoor and Mobile Radio Communications, PIMRC-95*, 140–143, Toronto, Canada, September 195.
10. Lee, W. C. Y. and D. J. Y. Lee, "Microcell prediction in dense urban area," *IEEE Transactions on Vehicular Technology*, Vol. 47, No. 1, 246–253, February 1998.

11. Okumura, Y., E. Ohmori, T. Kawano, and K. Fukuda, "Field strength and its variability in VHF and UHF land mobile radio services," *Review of the Electrical Communications Laboratory*, Vol. 16, 825–873, September–October 1968.
12. Hata, M., "Empirical formula for propagation loss in land mobile radio services," *IEEE Transactions on Vehicular Technology*, Vol. 29, No. 3, 317–325, September 1981.
13. COST Action 231, "Digital mobile radio towards future generation systems," *Final Report*, European Commission, No. 18957, 1999.
14. Electronic Communication Committee (ECC) within the European Conference of Postal and Telecommunications Administration (CEPT), "The analysis of the coexistence of FWA cells in the 3.4–3.8 GHz band," *ECC Report 33*, May 2003.
15. Rappaport, T. S., *Wireless Communications: Principles and Practice*, Prentice Hall, New Jersey, USA, 2002.
16. Wireless World Initiative New Radio (WINNER), 6th Framework Programme, Information Society Technologies, IST-2003-507591, Website: https://www.ist-winner.org/
17. The Working Group for WLAN Standards (IEEE 802.11), Website: http://www.ieee802.org/11/.
18. 3rd Generation Partnership Project, Website: http://www.3gpp.org/.
19. Papantoniou, S. J., "Modelling the mobile-radio channel," Ph.D. Thesis, No. 9120, ETH Zürich, 1990.
20. Fleury, B. and U. B. R. Heddergott, "Advanced radio channel model for magic WAND," ACTS Mobile Telecommunications Summit, 600–607, November 1996, Granada, Spain.
21. Nielsen, J. Ø., V. Afanassiev, and J. B. Andersen, "A dynamic model of the indoor channel," *Wireless Personal Communications*, Vol. 19, No. 2, 91–120, November 2001.
22. Chong, C. C., D. I. Laurenson, and S. McLaughlin, "The implementation and evaluation of a novel wideband dynamic directional indoor channel model based on a markov process," *14th IEEE Proceedings on Personal, Indoor and Mobile Radio Communications*, Vol. 1, 670–674, September 2003.
23. Wireless Local Area Network Hotspot Directory, W-Squared Inc., Website: http://www.wifi411.com/.
24. Calcev, G., D. Chizhik, B. Goransson, S. Howard, H. Huang, A. Kogiantis, A. F. Molisch, A. L. Moustakas, D. Reed, and X. Hao, "A wideband spatial channel model for system-

wide simulations," *IEEE Transactions on Vehicular Technology*, Vol. 56, No. 2, 389–403, March 2007.

25. 3GPP, "Spatial channel model for MIMO simulations," ftp://ftp.3gpp2.org/TSGC/Working/2001/TSG-C_0108/TSG-C-0801-Portland/WG5/.
26. WINNER II Channel Models, September 30, 2007, http://www.ist-winner.org/WINNER2-Deliverables/D1.1.2v1.1.pdf.
27. DeLange, O. E., "Propagation studies at microwave frequency by means of very short pulse," *Bell System Technical Journal*, Vol. 31, 91–103, January 1952.
28. Hewitt, A. and E. Vilar, "Sective fading on LOS microware links: Classical and spread_spectrum measurements techniques," *IEEE Trans. on Comms.*, Vol. 36, No. 7, 789–796, July 1988.
29. Crawford, A. B. and W. C. Jakes, "Selective fading of microwaves," *Bell System Technical Journal*, Vol. 31, 68–90, January 1952.
30. Bailey, R. J. and G. R. Summers, "Radio channel characterisation for the digital european cordless telecommunications system," *British Telecommunications Technology Journal*, Vol. 8, No. 1, 25–30, January 1990.
31. Turin, G. L., F. D. Clapp, T. L. Johnson, S. B. Fine, and D. Lavry, "A statistical model of urban multipath propagation," *IEEE Transactions on Vehicular Technology*, Vol. 21, No. 1, 1–9, February 1972.
32. Falconer, D. D. and S. Lek Ariyavisitakul, "Broadband wireless using singal carrier and frequency domain equalization," *5th International Symposium on Wireless Personal Multimedia Communications*, Vol. 1, 27–36, Honolulu, HI, USA, October 2002,.
33. Matic, D. M., H. Harada, and R. Prasad, "Indoor and outdoor frequency measurements for MM-waves in the range of 60 GHz," *48th IEEE Vehicular Technology Conference: Pathway to a Global Wireless Revolution*, Vol. 1, 567–571, Ottawa, Canada, May 1998.
34. Bajwa, A. S. and J. D. Parsons, "Small-area characterization of UHF urban and suburban mobile radio propagation," *IEE Proceedings*, Vol. 129, No. 2, 102–109, April 1982.
35. Godfrey, K., *Perturbation Signals for System Identification*, Prentice-Hall, London, UK, 1993.
36. Ditmar, W. P. A., M. Khoshlahjeh-Motamed, and R. R. Pettitt, "Design and Application of multi-frequency signals for power plant indentification," *IEE International Conference on Control'91*, Vol. 1, 665–670, Edinburgh, United Kingdom, March 25–28, 1991.

37. Nielson, D. L., "Microwave propagation measurements for mobile digital radio application," *IEEE Transactions on Vehicular Technology*, Vol. 27, No. 3, 117–131, August 1978.
38. Martin, G. T. and M. Faulkner, "Delay spread measurements at 1890 MHz in pedestrian areas of the central business district in the city of melbourne," *44th IEEE Vehicular Technology Conference*, Vol. 1, 145–149, Stockholm, Sweden, June 1994.
39. Cox, D. C., "Delay-doppler characteristics of multipath delay spread and average excess delay for 910 MHz urban mobile radio paths," *IEEE Transactions on Antennas and Propagation*, Vol. 20, No. 5, 625–635, September 1972.
40. Nche, C., A. M. D. Turkmani, and A. A. Arowojolu, "Channel sounder for PCN networks," *IEE Colloquium on High Bit Rate UHF/SHF Channel Sounders Technology and Measurements*, 5/1–6, Savoy Place, London, UK, December 1993.
41. Løvnes, G., S. E. Paulsen, and R. H. Rækken, "A millimeter wave channel sounder based on chirp/correlation technique," *IEE Colloquium on High Bit Rate UHF/SHF Channel Sounders Technology and Measurements*, 8/1–7, Savoy Place, London, UK, December 1993.
42. Salous, S. and V. Hinostroza, "Bi-dynamic indoor measurements with high resolution channel sounder," *5th International Symposium on Wireless Personal Multimedia Communications*, Vol. 1, 262–266, Honolulu, HI, USA, October 2002.
43. RUSK Channel Sounder Ordering Information, MEDAV GmbH, Website: http://www.channelsounder.de/.
44. Trulove, J., *Build Your Own Wireless LAN*, McGraw-Hill, New York, USA, 2002.
45. Duet Channel Sounder Technical Description, Berkeley Varitronics Systems, Inc., Website: http://www.bvsystems.com/Products/CDMA/Duet/duet.htm.
46. Elektrobit Propsound Channel Sounder Technical Description, Elektrobit Corporation, Website: http://www.elektrobit.com/index.php?209.
47. Van Rees, J., "Measurements of the wideband radio channel characteristics for rural, residental, and suburban areas," *IEEE Transactions on Vehicular Technology*, Vol. 36, No. 1, 2–6, February 1987.
48. Safer, H., G. L. Berger, and F. Seifert, "Propagation measurement-based probability of error predictions for the tactical VHF-range," *IEEE Military Communication Conference Proceed-*

ings, 331–335, November 1999.

49. Dinis, M. and J. Fernandes, "Provision of sufficient transmission capacity for broadband mobile multimedia: A step toward 4G," *IEEE Comm. Magazine*, Vol. 39, No. 8, 46–54, August 2001.
50. Austin, J., W. P. A. Ditmar, W. K. Lam, E. Vilar, and K. W. Wan, "A spread spectrum communication channel sounder," *IEEE Transactions on Communications*, Vol. 45, No. 7, 840–847, July 1997.
51. Hunt Engineering, "Choosing FPGA or DSP for your application," 2010, http://www.hunteng.co.uk/info/fpga-or-dsp.htm.
52. Parker, M., "FPGA versus DSP design reliability and maintenance," 2010, http://www.dsp-fpga.com/articles/id/?2207.
53. Bilsby, D. C. M., R. L. Walke, and R. W. M. Smith, "Comparison of a programmable DSP and a FPGA for real-time multiscale convolution," *IEE Colloquium on High Performance Architectures for Real-Time Image Processing*, No. 1998/197, 4/1–4/6, London, February 1998.
54. Analog Devices, "AD12401 data sheet," 2010, http://www.analog.com/en/analog-to-digital-converters/ad-converters/ad12401/products/product.html.
55. Technobox Inc., "64-bit PMC-to-PCI adapter card data sheet," 2010, Website: http://www.technobox.com/cat3673.pdf.
56. Alpha Data Ltd., "ADM-XRC-II xilinx virtex-II PMC data sheet," Alpha Data, 2010, Website: http://www.alpha-data.com/adm-xrc-ii.html.
57. Torres, R. P., B. Cobo, D. Mavares, F. Medina, S. Loredo, and M. Engels, "Measurement and statistical analysis of the temporal variations of a fixed wireless link at 3.5 GHz," *Wireless Personal Communications*, Vol. 37, Nos. 1–2, 41–59, April 2006.
58. Ikegami, F., S. Yoshida, T. Takeuchi, and M. Umehira, "Propagation factors controlling mean field strength on urban streets," *IEEE Transactions Antennas and Propagation*, Vol. 32, No. 8, 936–942, August 1984.
59. Feuerstein, M. J., K. L. Blackard, T. S. Rappaport, S. Y. Seidel, and H. H. Xia, "Path loss, delay spread, and outage models as functions of antenna height for microcellular system design," *IEEE Transactions on Vehicular Technology*, Vol. 43, No. 3, 487–498, August 1994.
60. Walfisch, J. and H. Bertoni, "A theoretical model of UHF propagation in urban environments," *IEEE Transactions Antennas and Propagation*, Vol. 36, No. 12, 1788–1796, December 1988.